PARTICLE SIZE DETERMINATION FROM LOCAL FALLOUT

THESIS

Norman C. Davis
Captain USMC

AFIT/GNE/ENP/86D-1

DEPARTMENT OF THE AIR FORCE
AIR UNIVERSITY
AIR FORCE INSTITUTE OF TECHNOLOGY

Wright-Patterson Air Force Base, Ohio

AFIT/GNE/ENP/86D-1

PARTICLE SIZE DETERMINATION FROM LOCAL FALLOUT

THESIS

Norman C. Davis
Captain USMC

AFIT/GNE/ENP/86D-1

AFIT/GNE/ENP/86D-1

PARTICLE SIZE DETERMINATION FROM LOCAL FALLOUT

THESIS

Presented to the Faculty of the School of Engineering

of the Air Force Institute of Technology

Air University

In Partial Fulfillment of the

Requirements for the Degree of

Master of Science in Nuclear Engineering

Norman C. Davis

Captain, U. S. Marine Corps

December 1986

Approved for public release; distribution unlimited

Acknowledgement

I would like to thank Dr. Charles J. Bridgman for his advice and support during the course of this thesis research. His familiarity with this subject was of tremendous assistance. I would also like to thank George H. Baker, an AFIT doctoral student, whose own research was a valuable source of ideas for this project.

Norman C. Davis

Contents

Contents

List of Figures

List of Tables

Abstract

The purpose of this research was to examine iso-dose rate contours and cloud arrival time data from atmospheric nuclear tests conducted at the Nevada Test Site to validate size distributions currently used in fallout prediction models or to propose new size distributions. Results were obtained from studies of eight air, nine tower, two surface and two shallow subsurface bursts. Yields ranged from 0.3 to 74 kilotons and heights of burst ranged from -67 to 1500 feet. The tests examined are tabulated in Appendix A.

Iso-dose rate contours from U. S. atmospheric nuclear tests (9) were digitized and then integrated numerically to obtain information on the fraction of activity grounded with time. The parameters of the best-fit lognormal and best-fit power-law particle-size distributions were then found for each burst studied.

There was insufficient fallout from tower and air bursts to make conclusive determinations about the size distributions produced by these classes of bursts. For surface and shallow subsurface bursts the debris may be characterized by a lognormal distribution, by a power-law r^n distribution, or by a linear combination of these or possibly other distribution functions. While no definitive distribution function was established, a linear combination of lognormal distributions seems to hold the most promise. In addition, a lower bound of 2210 r-mi^2/hr-kt was established for the source normalization constant.

DETERMINATION OF PARTICLE SIZE DISTRIBUTION FROM LOCAL FALLOUT

I. Introduction

The size distribution of debris produced by nuclear explosions has been the subject of much study. This distribution is essential to the prediction of local fallout in tactical planning and the extent of global fallout that would be produced by high-yield strategic weapons. The degree of sunlight attenuation and subsequent climate pertubation predicted by the nuclear winter hypothesis is also acutely sensitive to this size distribution.

Determinations of particle size distribution have been based on optical measurement of nuclear debris (15) and measurement of specific activity as a function of particle size (11). These microscopic methods are advantageous because they are based on measurements of real particles produced by bursts that occurred under known conditions. However, there are several significant disadvantages to these methods. In the case of air samples, the time and location of sampling will greatly affect the apparent size distribution of particles collected (2). Ground sampling stations at different locations will collect particles of different sizes with larger particles tending to fall out closer to ground-zero (13:81). Correcting for these sampling biases is not an easy task. Methods that use activity to determine particle size distributions are further complicated by the fractionation phenomena (6).

This research attempts to utilize the local fallout data from U. S. atmospheric nuclear tests to determine a number-size distribution for fallout particles. It is a macroscopic approach in that the particle size distribution of the nuclear cloud is found from the aggregate

behavior of the entire radioactive cloud rather than samples that are representative of only a portion of that cloud.

Three proposed particle size distributions are described in Chapter II. The method utilized in this research to obtain particle number-size distributions from the fallout data is outlined in Chapter III. Fractionation and the source normalization constant are discussed in Chapter IV. The results of this research are presented in Chapter V. Conclusions and recommendations are presented in Chapter VI.

II. Particle Size Distributions

Several particle number-size distributions have been proposed to represent nuclear bomb debris. Three such distributions are presented in this chapter. These are the lognormal distribution, power-law distribution and the hybrid distribution. It will be shown that the latter distribution is really just a combination of the first two. The relationship between the number-size distribution and the activity-size distribution is also examined in this chapter.

Lognormal Distributions

The number-size density function describing debris particles produced by nuclear explosions has been taken to be lognormal where the fraction of particles n (r) between radius r and r + dr is given by

$$n(r)\,dr = \frac{1}{\sqrt{2\pi}} \exp\left[-1/2 \left(\{ \ln r - \ln r_m \} / \beta \right)^2 \right] \frac{d(\ln r)}{\beta} \qquad (1)$$

where r_m is the median radius of the number-size distribution and β is the slope, or geometric standard deviation, of the distribution. Nathans et al have developed a theoretical basis for this distribution by applying the theory of self-preserving size distributions to particle formation after nuclear air bursts (16).

If the activity is distributed on the surface of the fallout particles, as might be expected for fission products with more volatile precursors, then the surface activity-size distribution, a_s (r), is given by

$$\begin{aligned} a_s(r)\,dr &= A_{so}\,\rho_s\,4\pi r^2\,n(r)\,dr \\ &= \frac{1}{\sqrt{2\pi}} \exp\left[-1/2 \left(\{ \ln r - \ln r_s \} / \beta \right)^2 \right] \frac{d(\ln r)}{\beta} \end{aligned} \qquad (2)$$

(4:210), where ρ_s is the surface activity density and A_{so} normalizes the distribution so that

$$\int_0^\infty a_s(r)\,dr = 1. \tag{3}$$

The surface activity-size distribution, $a_s(r)$, is then the second moment of the number-size distribution. This distribution is also lognormal (1:12) with median radius, r_s, given by

$$r_s = r_m \exp[\,2\beta^2\,]. \tag{4}$$

If the activity is volume-distributed, as might be the case for refractory fission products, then the volume activity-size distribution, $a_v(r)$, is given by

$$a_v(r)\,dr = A_{vo}\,\rho_v\,(4\pi/3)\,r^3\,n(r)\,dr$$

$$= \frac{1}{\sqrt{2\pi}} \exp[\,-1/2\,(\{\ln r - \ln r_v\}/\beta)^2\,]\,\frac{d(\ln r)}{\beta} \tag{5}$$

where ρ_v is volume activity density and A_{vo} normalizes $a_v(r)$ in a similar manner as A_{so} normalizes $a_s(r)$ in equation (3). The volume activity-size distribution is the third moment of the number-size distribution with median radius, r_v, given by

$$r_v = r_m \exp[\,3\beta^2\,]. \tag{6}$$

In general, the n-th moment of the number-size distribution will itself be lognormal (1:12) with median radius, r_n, given by

$$r_n = r_m \exp[\,n\beta^2\,]. \tag{7}$$

Freiling suggested the activity-size distribution function could, for each mass chain, be described by a single lognormal distribution with a median radius given by

$$r_{mk} = r_m \exp [(2 + b_k) \beta^2]. \quad (8)$$

where r_{mk} is the median radius of the activity distribution for mass chain k and b_k is a number that is almost invariably between 0 and 1 (8:10). Comparison of equations (4), (6) and (8) shows that a b_k of 0 corresponds to surface-distributed activity and a b_k of 1 corresponds to volume-distributed activity. The Department of Defense Land Fallout Prediction System (DELFIC) uses this radial distribution model to obtain an activity distribution by summing over the significant mass chains weighted according to the fraction of that chain produced by the burst (18). Note carefully that this linear combination of lognormal distributions results in a distribution that is not itself lognormal.

Bridgman and Bigelow simplified the DELFIC model to represent the activity-size distribution by a linear combination of two lognormal distributions

$$a (r) = f_v a_v (r) + (1 - f_v) a_s (r) \quad (9)$$

where f_v is the fraction of the activity that is volume distributed (4:211). They demonstrated graphically how this combination of lognormal distributions compares to the volume and surface activity distributions for the DELFIC default particle size distribution (Table 1) with $f_v = 0.68$ and to the DELFIC model itself (4:211).

To further simplify calculations, the activity-size distribution might be approximated by a single lognormal distribution (3), a (r), with median radius, $r_{2.5}$, given by

$$r_{2.5} = r_m \exp [2.5 \beta^2]. \quad (10)$$

As shown in Figure 1, this simplified distribution lies midway between the surface and

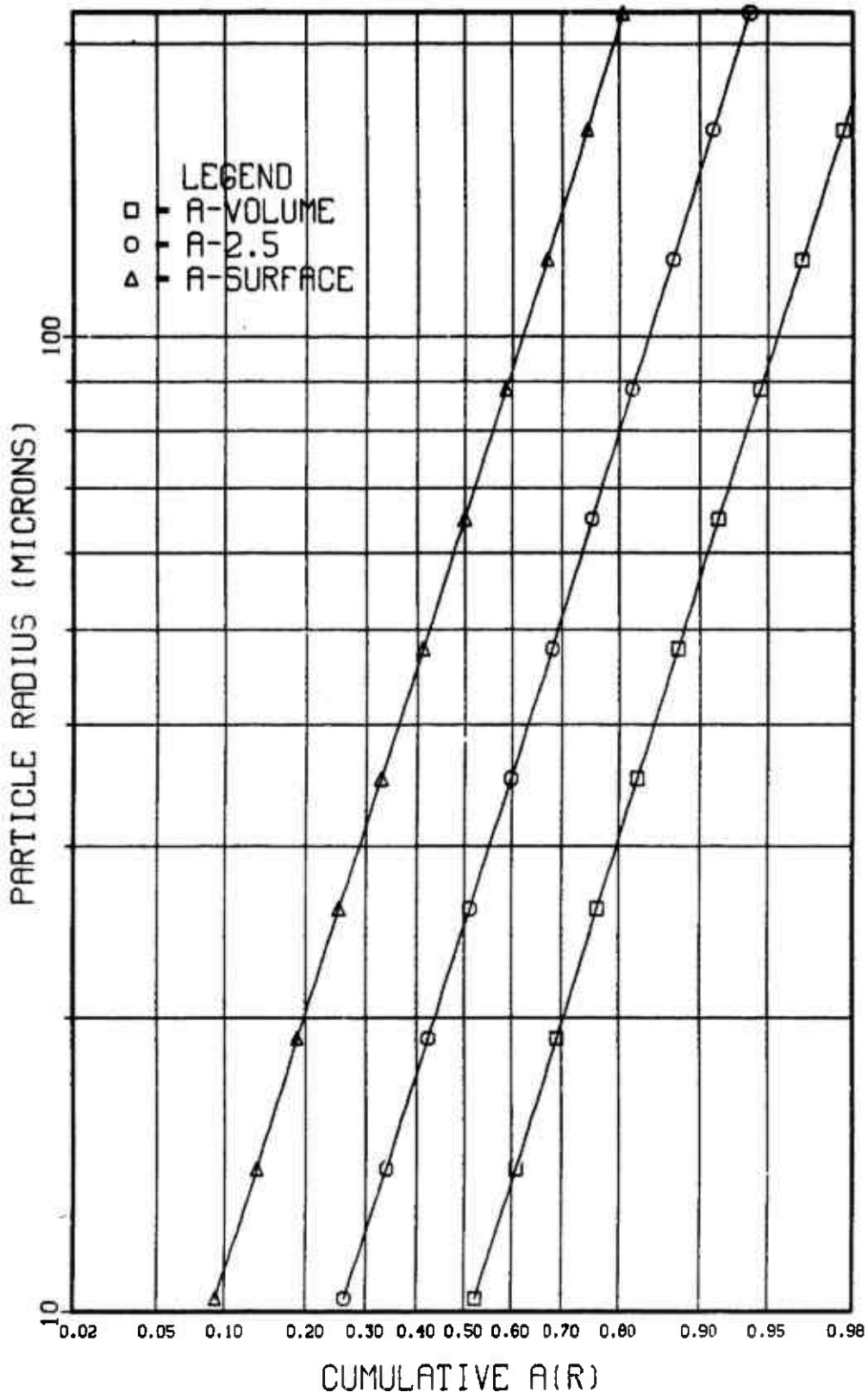

Figure 1: Comparison of Activity-Size Distribution Models

volume activity distributions.

Heft suggested that nuclear debris may be described by a linear combination of several lognormal distributions, one such distribution for each type of particle generated by the burst (11:254). Yoon claimed that at scaled heights of burst above 700 feet a significant mass of soil is no longer entrained in the fireball (23:3-6). This height is given by

$$SHOB = HOB \times Y^{-1/3} \tag{11}$$

where Y is the yield of the weapon in kilotons and both the scaled height of burst, SHOB, and height of burst, HOB, are in feet. Air bursts at or above this height may be described by a single lognormal distribution. Heft proposed that surface bursts, tower bursts and air bursts where soil is entrained in the fireball might be described by a linear combination of two lognormal distribution functions, one to represent the device debris and vaporized soil, a_t, and one to represent completely or partially melted soil and tower materials, a_2 (11:254). The cumulative activity-size distribution, A (r), which is simply the fraction of activity carried by particles of radius less than r, is then given by

$$A(r) = f_1 \int_0^r a_1(r')\,dr' + f_2 \int_0^r a_2(r')\,dr' \tag{12}$$

where $f_1 + f_2 = 1$ and $a_i(r')$ is related to $n_i(r)$ as in equation (10).

Subsurface bursts might be described by a linear combination of three lognormal distributions. The third component seems to result "from soil material which interacted with the fireball at high temperature but which was separated from the fireball early" (11:256). In this case

$$A(r) = f_1 \int_0^r a_1(r')\,dr' + f_2 \int_0^r a_2(r')\,dr' + f_3 \int_0^r a_3(r')\,dr' \tag{13}$$

where $f_1 + f_2 + f_3 = 1$.

Power-Law Distribution

Another number-size distribution function is the power-law distribution. Russell suggested the activity-mass distribution in prompt fallout is roughly a constant over a wide range of particle sizes (7:4). This is equivalent to an r^{-3} number-size relationship. To generalize this power-law relationship the number-size density function may be given by

$$n(r)\,dr = N_o\, r^{n}\, dr \tag{14}$$

where N_o is a normalization constant. If n is positive then a minimum radius, r_{min}, is required to keep n (r) finite as r approaches zero. If $n \leq 4$ then a maximum radius, r_{max}, is required in order to normalize the mass-size distribution, the third moment of the number-size distribution.

Equations (4) and (6) representing the surface and volume activity-size distributions respectively are equally valid for the power-law distribution. Equation (14) is used for n (r). These activity-size distributions may be normalized as in equation (3) by noting that n (r) = 0 when $r > r_{max}$ or $r < r_{min}$. Equations (12) and (13) describing multiple distributions are also valid for power-law distributions.

In general the cumulative activity-size distribution, A (r), for the k-th moment of the power-law distribution, $n \neq k + 1$, is given by

$$A(r) = \kappa \left[r^{k-n+1} - r_{min}^{\,k-n+1} \right] \tag{15a}$$

where $\kappa = \left[r_{max}^{\,k-n+1} - r_{min}^{\,k-n+1} \right]$ is a normalization constant. When $n = k + 1$,

$$A(r) = \kappa \ln \left[r / r_{min} \right] \tag{15b}$$

where now $\kappa = \ln [r_{max} / r_{min}]$ is the normalization constant.

Hybrid Distribution

The particle size distribution may be given as a hybrid distribution described by a lognormal distribution below a given radius, r_o, and a power-law distribution above that radius. When $r < r_o$,

$$n(r)\,dr = N_o (r_m / r) (r_o / r_m)^{(n+1)/2} \exp [-1/2 (\{ \ln r - \ln r_m \} / \beta)^2]\, dr \quad (16a)$$

and when $r_o \geq r \geq r_{max}$,

$$n(r)\,dr = N_o (r / r_o)^{-n}\, dr \quad (16b)$$

(20:21). N_o is a normalization constant. The transition radius, r_o, may be found by requiring that the number-size distribution and its first derivative be continuous at r_o. This radius is given by

$$r_o = r_m \exp [(n-1) \beta^2]. \quad (17)$$

Once again, if $n \leq 4$, a maximum radius, r_{max}, is required to normalize the mass distribution. This radius is given by

$$r_{max} = r_o \exp [\sqrt{2\pi}\, \beta (1 - f_m) / 2 f_m] \quad (18)$$

where f_m is the fraction of mass carried by particles smaller than r_o. Once again equations (4), (6), (12) and (13) are also valid for this distribution.

Parameters of Proposed Distributions

A number of single lognormal particle size distributions have been proposed for Nevada soil. These are summarized in Table 1. Note that while these distributions propose very different values for the parameters r_m and β, they predict values for $r_{2.5}$ over a relatively narrow range spanning less than a decade on a logarithmic scale. As shown in Figure 1, a single lognormal distribution which is the 5/2 moment of the number-size distribution, n (r), is an approximatôn of a (r). Cumulative log-probability plots of these proposed lognormal distributions are shown in Figure 2.

Parameters have been proposed for other distributions. Russell suggested a power-law distribution with an exponent of 3 (7:4). Nathans has suggested that the size distribution is a hybrid distribution that is lognormal below about 3 μ while obeying a power-law with an exponent between 3.3 and 4.4 from 3 to about 70 μ (15:360,370). Turco et al adapted a hybrid distribution from Nathan's work with a lognormal median radius of 0.25 μ, slope of ln 2 and a power-law tail with an exponent of 4. They chose f_m to be 0.084 (20:21).

Table 1: Proposed Lognormal Parameters
Nevada Soil

	Median Radius, r_m (μ)	exp (β)	Activity Median, $r_{2.5}$ (μ)†
NRDL-N61	0.0039	7.24	70.1
NRDL-D	0.01	5.42	12.6
DELFIC	0.204	4	24.9
WESG	10.6	2	35.2
Huebsch (3)	0.021	5.42	26.5
Henriques & Richards (3)	0.16	4.48	44.2

Source: Reference (5:11) except where otherwise noted.

† Calculated from equation (10).

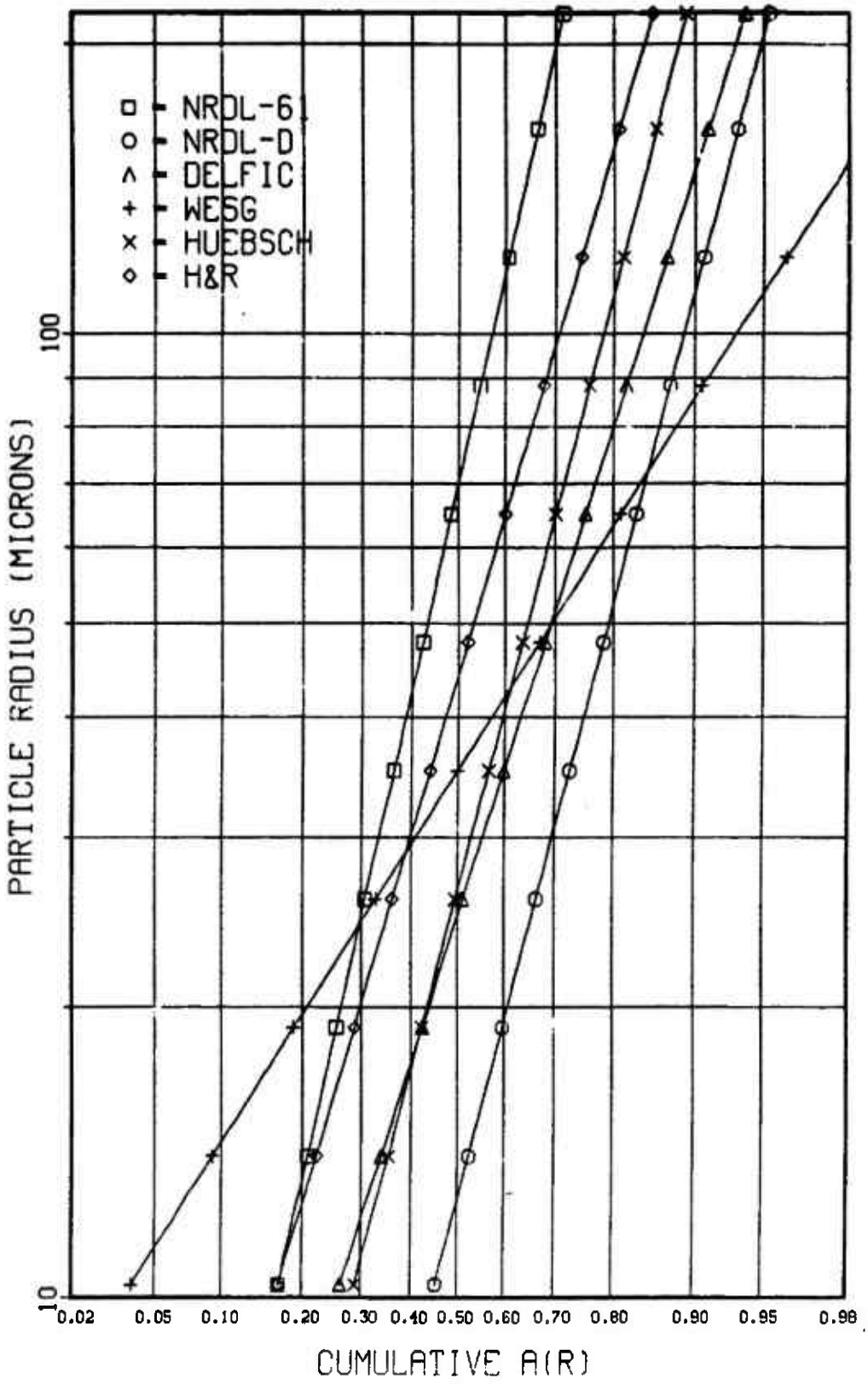

Figure 2: Proposed Lognormal Activity-Size Distributions for Nevada Soil

III. Method

In this chapter we will examine the method utilized in this study to determine which, if any, of the particle size distributions discussed in Chapter II best describe the local fallout data. The emphasis will be on the lognormal and power-law distributions. These methods may be applied to the hybrid distribution though the computations required to obtain the parameters of that distribution are much more difficult.

Contour Integration

The on- and off-site iso-dose rate contours and arrival time curves from reference (10) were digitized to permit integration of total activity grounded to successive arrival time curves. The on- and off-site iso-dose rate contours were integrated to successive arrival times to give J (t) in r-mi^2/hr. It will be shown that this quantity is proportional to the amount of activity grounded at time t. The integration was trapezoidal, linearly interpolating between contours. Examples of on- and off-site iso-dose rate contours for Operation BUSTER-JANGLE Sugar are shown in Figures 3 and 4 (10:56-57).

Another technique has been used to integrate fallout contours. Tompkins (19) and others have found J from

$$J = \int_{-\infty}^{\ln(I_{max})} A(I)\, I\, d(\ln I) \qquad (19)$$

where A (I) is the area enclosed by the iso-dose contour of intensity I and I_{max} is the maximum intensity in the fallout field. J is obtained graphically by plotting the product A (I) I versus ln I. J is then simply the area enclosed by this curve. While this method might produce more reliable results, it was not appropriate for this study because it does not permit

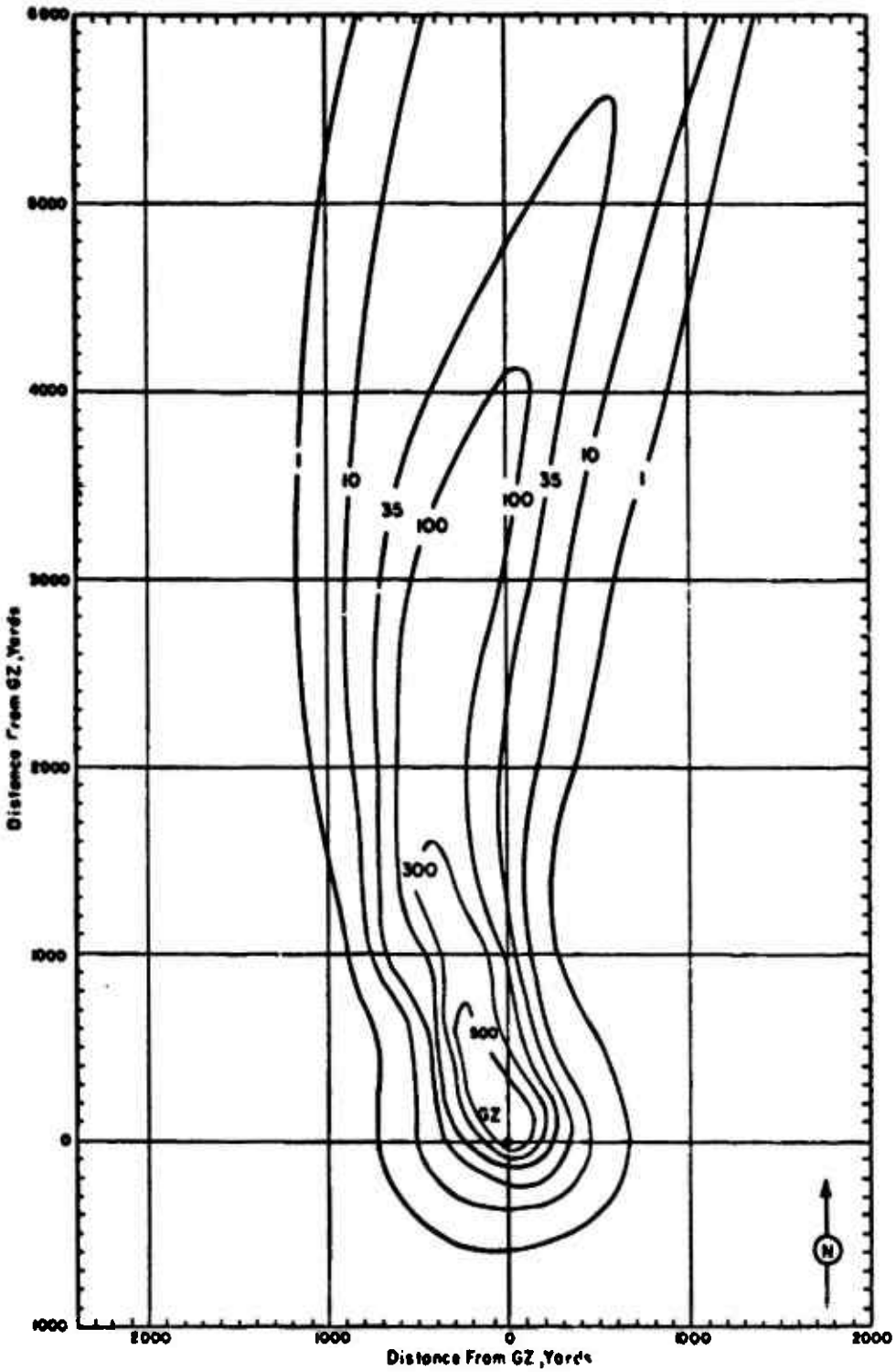

Figure 3: On-Site Iso-Dose Rate Contours
BUSTER-JANGLE Sugar

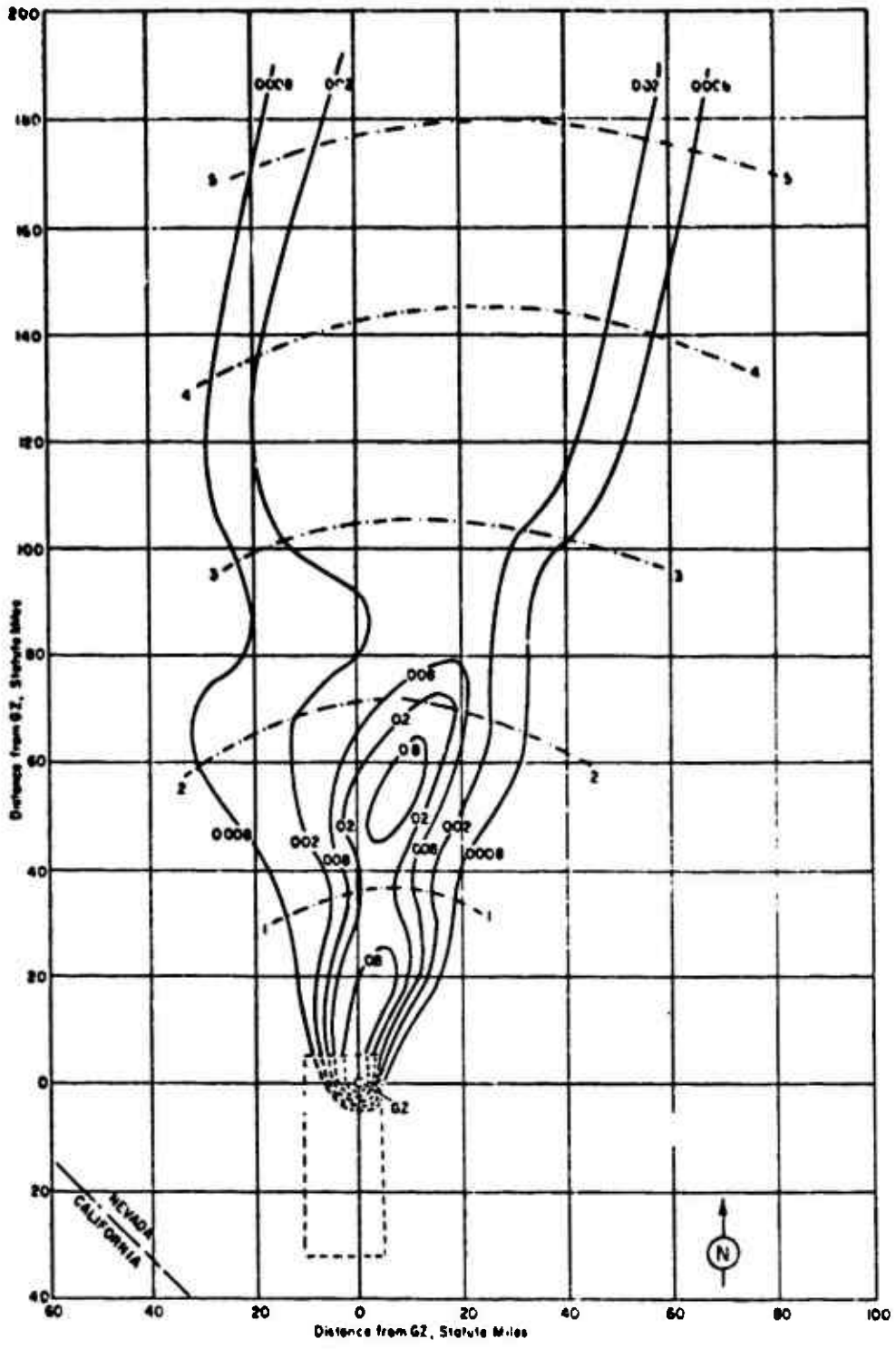

Figure 4: Off-Site Iso-Dose Rate Contours
BUSTER-JANGLE Sugar

determination of the time-dependence of the fallout.

J (t), G (t) and A [r (t)]

The result of the contour integration, J (t), might be thought of as the dose rate that would be measured at one hour after the burst three feet above the center of a one-square mile area if all the activity grounded at time t were distributed uniformly over that area. This quantity is divided by the yield of the weapon in kilotons and an effective source normalization constant to give the fraction of activity grounded as a function of time, G (t). These results are presented in Appendix B.

G (t) can be translated into A [r (t)], the fraction of activity carried by particles of radius less than r, also called the cumulative activity-size distribution, by noting that, with the assumptions below,

$$G(t) = \int_0^t g(t')\,dt' = 1 - A[r(t)] = \int_{r(t)}^{\infty} a(r)\,dr \qquad (20)$$

(3,4:207,210) where g (t') is the fractional rate of activity arrival on the ground at time t' and a (r) is the activity-size density function.

Assumptions

A number of assumptions were made in this study in order to extract a particle number-size distribution from the local fallout data. These assumptions are:

1. The altitude of activity lofted into the stabilized cloud is the bottom of the visible cloud. In several instances this had to be estimated from the available cloud top height and the dimensions of clouds produced by similar bursts.

2. The mean elevation of the Nevada Test Site, the elevation at wnich particles

grounded, was taken to be 1200 meters.

3. Particles fell through a U. S. Standard Atmosphere (21,22:2-9) with the velocity predicted for spherical particles by Davies-MacDonald fall mechanics (4:212) in the absence of vertical air movement.

4. At time t when particles with radius r (t) are grounding, all particles with radii greater than r (t) are on the ground and all particles with radii less than r (t) are not. This is the "pancake cloud" approximation.

5. All activity inside a given arrival time curve grounded before that time and all activity outside that arrival time curve grounded after that time.

6. Unless stated to the contrary in reference (10), neutron-induced radiation did not contribute significantly to on-site dose rates. If the on-site activity was noted to be primarily due to neutron-induced radiation, then 10% of the on-site activity was assumed to be due to the fission products.

7. The source normalization constant was taken to be 2350 r-mi^2/hr-kt (4:208). Fractionation is not treated explicitly.

8. The activity-size distribution is approximated by the 5/2 moment of the number-size distribution (3).

Taken together these assumptions result in a two-dimensional cloud that becomes stratified according to particle size. The particles sediment under the influence of gravity and horizontal winds such that successively smaller particles are grounding at increasing times t. These approximations are least valid at early times when cloud growth and other hydrodynamic processes dominate particle motion. They are most valid when the downwind distance exceeds about two cloud diameters (4:215).

Parameters of Lognormal Distributions

The lognormal distribution may be transformed into the better known normal distribution

by substituting $z(t) = [\ln r(t) - \ln r_{2.5}] / \beta$ into Equation (20) with a (r) given by

$$a(r)\,dr = \frac{1}{\sqrt{2\pi}} \exp\left[-1/2\left(\{\ln r - \ln r_{2.5}\}/\beta\right)^2\right] \frac{d(\ln r)}{\beta}. \qquad (21)$$

The fraction of activity carried by particles larger than those grounding at time t, A [r (t)], then becomes

$$A[r(t)] = \int_{-\infty}^{z(t)} \frac{1}{\sqrt{2\pi}} \exp\left[-1/2\, z^2\right] dz \qquad (22)$$

This is simply the cumulative normal function. Since A [r (t)] is known for each time t, the value of the upper limit of integration may be found (12:MDNRIS-1). The values of the parameters $r_{2.5}$ and β are then found from a linear least-squares fit, of the data in Appendix B, of the form

$$y = mx + b \qquad (23)$$

where y is z (t), x is ln r (t), m is $1 / \beta$ and b is $- \ln r_{2.5} / \beta$.

A linear combination of two lognormal distributions is defined by five parameters (r_{m1}, β_1, r_{m2}, β_2, f_1). If the parameters of one distribution and the partition of activity between the two distributions are fixed, then the parameters of the second distribution may be readily found. Baker's proposed distribution for long-term stratospheric activity-bearing debris, r_{m1} of 0.1 μ and β_1 of ln 2 (2), was chosen to represent the device debris, n_1 (r). By varying the fraction of activity carried by these particles, f_1, a set of parameters to describe the second distribution, n_2 (r), may be found by the method outlined previously by noting that

$$A_2 [r(t)] = 1 - [\{ G(t) - f_1 \int_{r(t)}^{\infty} a_1 (r)\, dr \} / f_2] \qquad (24)$$

It is important to note that a different r_{m2} and β_2 will be found for each choice of r_{m1}, β_1 and f_2.

Parameters of Other Distributions

Parameters of other distribution functions cannot be found as easily as the parameters of the lognormal distribution. Fitting these other distributions requires varying the parameters of the chosen distribution until the best agreement with the data is achieved. Since the uncertainty in the data is so great and there are so many parameters to be determined, this parameter variation will often result in more than one possible set of parameters for each test examined.

The power-law distribution may be fit to the data by using equations (15) with k = 2.5, assumption (8), to find that, when $n \neq 3.5$,

$$1 - G(t) = A [r(t)] = \kappa [r(t)^{3.5-n} - r_{min}^{3.5-n}] \qquad (25a)$$

where $\kappa = (r_{max}^{3.5-n} - r_{min}^{3.5-n})^{-1}$ is a normalization constant. When n = 3.5,

$$1 - G(t) = A [r(t)] = \kappa' \ln [r(t) / r_{min}] \qquad (25b)$$

where now $\kappa' = \ln [r_{max} / r_{min}]$ is the normalization constant. Nathans in his studies of nuclear air burst debris rarely observed particles smaller than 0.01 μ (14). This value was chosen for r_{min}. The remaining parameters, r_{max} and n, were varied until best agreement with the data was found. This was done by minimizing a figure of merit given by

$$\text{fom} = \sum_{i=1}^{N} | A [r (t_i)]_{data} - A [r (t_i)]_{calc} | \qquad (26)$$

where N is the number of data for the test under consideration and $A [r (t_i)]_{calc}$ is calculted using the selected values for the parameters n and r_{max}. The parameters of the hybrid distribution, r_m, β, f_m and n, may be found by varying these parameters in a similar manner.

Discussion

There are advantages and disadvantages to this local fallout, or macroscopic, approach to particle size distribution determination. The most important advantage of this method is there are no sampling or counting biases to be corrected for. It is based on the activity measured on the ground for a number of atmospheric nuclear tests. There are, however, several significant disadvantages to this method.

The off-site iso-dose contours were often based on a limited number of measurements and are therefore less reliable than the on-site contours. This is significant because, as can be seen in Figure 4, the time-dependence of the activity deposition is obtained primarily from the off-site contours. Another source of uncertainty is the arrival time curves. These were not based on detailed observations of the cloud or the observed onset of activity arrival on the ground. They were computed from wind data and available monitoring information and are intended to give only a rough average of arrival time (10:3).

The most severe limitation is that this method attempts to postulate a particle size distribution indirectly, that is without actual measurements of fallout particles. Thus this approach cannot alone conclusively establish a particle size distribution. At best it can validate distributions that have been obtained by direct methods.

Lastly, a number of the assumptions that were made to obtain the desired information about the particle number-size distribution, particularly assumptions (4), (5) and (8), are

crude simplifications of the fallout physics. This model ignores the three-dimensional geometry of the radioactive cloud and many of the physical processes occurring during the rise and stabilization of the cloud. A more rigorous treatment certainly is possible, though computationally much more difficult. Such a treatment would also be limited by the tremendous uncertainty in the local fallout data. Thus confidence in the results would only be marginally improved.

IV. Source Normalization Constant

Definition

The fraction of activity grounded at time t, G (t), was found by dividing the result of the numerical integration of the iso-dose rate contours, J (t), in units of r-mi^2/hr, by an effective source normalization constant, K, and the yield of the device in kilotons. This constant is the dose rate that would be measured one hour after burst three feet above a smooth, one-square mile plane if all the activity from a one-kiloton fission device were spread uniformly over that surface (9:454). From this definition it may be seen that G (t) may also be called the "fraction of the device" (8:2) grounded at time t.

A surface roughness factor α, $\alpha \leq 1$, corrects for the reduction in dose rate caused by self-shielding over a real surface as compared to an ideal planar surface. The effective source normalization constant is related to the ideal value by

$$K = \alpha K_o \tag{27}$$

where K_o is the value of the constant for an ideal smooth surface.

Fractionation

This definition of source normalization constant is strictly valid only in the absence of fractionation. This is because fractionation may cause the fraction of one component of the debris that has fallen to ground at any time t to be different than the fraction of some other component of the debris. Freiling suggested the term "fraction of the device" could be replaced by the fraction of some component of the debris. One component is chosen as a reference and the abundance of other components is related to it. He chose the mass-95 chain as the reference component (8:2,8-9).

The model used in this study does not treat the fractionation phenomena explicitly. To do so would require adding many more variables to an already ill-posed problem. The correlation of relative isotopic abundance to particle size and yield of the device is poorly understood. The local fallout data used in this study is also not well-established. To treat fractionation explicitly would greatly complicate the size-distribution calculations without increasing the confidence in the results.

Lower Bound

A wide range of values for the source normalization constant have been reported. These are summarized in Table 2. Clearly this factor will have an impact on the computed fraction of activity grounded at any time. A lower bound on this constant may be found by noting that for Operation TEAPOT Ess G (10 hrs) was found to be 2213 r-mi^2/hr. Since the yield of this burst was 1 kiloton (10:201), the source normalization constant, K, must be at least 2213 r-mi^2/hr-kt.

Note that this lower bound is valid only for the Nevada Test Site or similar terrain. A different surface roughness factor, α, for another location would produce a different effective source normalization constant K.

Table 2: Source Normalization Constant
Surface Roughness Factor Included

	K_s (r-mi^2/hr-kt)
LRL-h	2700
Dropsy	2585
NREC	2500
WSEG	2400
DELFIC (4:208)	2350
Tompkins (19:10)	1725
RAND	1200
DIA	1100
NRDL-D	1093
USWB	1025

Source: Reference (17:18) except where otherwise noted.

V. Results

The results of the integration of the iso-dose rate contours to successive arrival times and the particle radii corresponding to these arrival times are presented in Appendix B. These results were analyzed using the methods outlined in Chapter III to find the parameters of lognormal and power-law distribution that best describe these data. The results are compared to the lognormal and power-law distributions presented in Chapter II.

Single Distribution

Lognormal distribution parameters for two air and two tower bursts are presented in Table 3. It should be noted that the remaining air and tower bursts may not reasonably be described by a single lognormal distribution. Clearly unreasonable median radii were found for the remaining bursts. For example, r_m for PLUMBBOB Priscilla is found by this method to be $4.6\times10^{-6}\,\mu$. This is smaller than the magnitude of atomic dimensions, an obviously a non-physical result. Power-law distribution parameters for these bursts are presented in Table 4.

The surface and subsurface bursts examined may be described by a single lognormal distribution as summarized in Table 3. The median radii of the activity distribution, $r_{2.5}$, found for shots BUSTER-JANGLE Sugar and Uncle are consistent with the proposed distributions for Nevada soil contained in Table 1. TEAPOT Ess may not be consistent because it was buried significantly deeper than was Uncle. These bursts may also be described by a power-law distribution. Table 4 shows these parameters for surface and subsurface bursts. Figures 5-7 show graphically how the lognormal and power-law distributions describe the data for TEAPOT Ess and BUSTER-JANGLE Uncle and Sugar.

Table 3: Lognormal Parameters
(Single Distribution)

	Median Radius, r_m (μ)	exp (β)	Activity Median, $r_{2.5}$ (μ)
Subsurface			
TEAPOT Ess	0.00045	10.5	470
BUSTER-JANGLE Uncle	1.1	3.6	70
Surface			
BUSTER-JANGLE Sugar	0.027	5.7	56
Tower			
TEAPOT Met	0.098	3.4	4.3
UPSHOT-KNOTHOLE Harry	0.069	3.8	5.9
Air			
HARDTACK II Lea	0.051	2.9	0.85
PLUMBBOB Doppler	0.0064	3.7	0.42

Table 4: Power-Law Parameters
(Single Distribution)

	Min Radius (μ)	Max Radius (μ)	Exponent
Subsurface			
TEAPOT Ess	0.01	510	2.75
BUSTER-JANGLE Uncle	0.01	100	2.35
Surface			
BUSTER-JANGLE Sugar	0.01	170	2.90
PLUMBBOB Coulomb B	0.01	900	3.45
Tower			
TEAPOT Hornet	0.01	550	3.70
TEAPOT Bee	0.01	380	3.85
TEAPOT Appie	0.01	340	3.90
PLUMBBOB Shasta	0.01	440	3.75
TEAPOT Met	0.01	130	3.75
UPSHOT-KNOTHOLE Nancy	0.01	440	3.80
TEAPOT Apple II	0.01	500	3.85
UPSHOT-KNOTHOLE Harry	0.01	120	3.60
UPSHOT-KNOTHOLE Simon	0.01	690	3.65
Air			
PLUMBBOB Lea	0.01	80	4.30
PLUMBBOB Morgan	0.01	300	4.15
PLUMBBOB Owens	0.01	160	4.15
PLUMBBOB Stokes	0.01	195	4.50
UPSHOT-KNOTHOLE Grable	0.01	190	4.20
PLUMBBOB Stokes	0.01	195	4.50
PLUMBBOB Priscilla	0.01	120	4.10
PLUMBBOB Hood	0.01	420	4.35

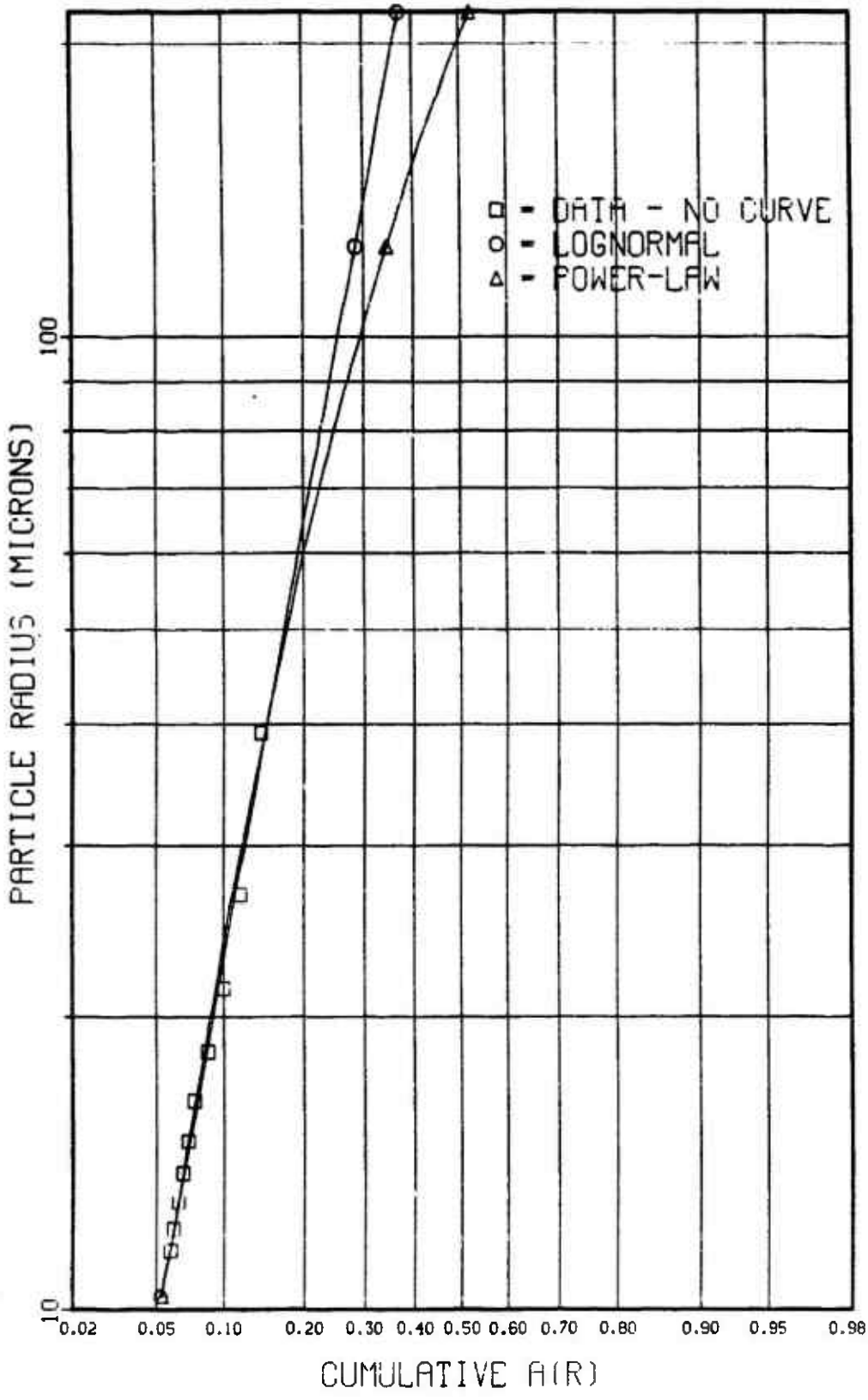

Figure 5: Lognormal and Power-Law Fits to Local Fallout Data
Operation TEAPOT Ess

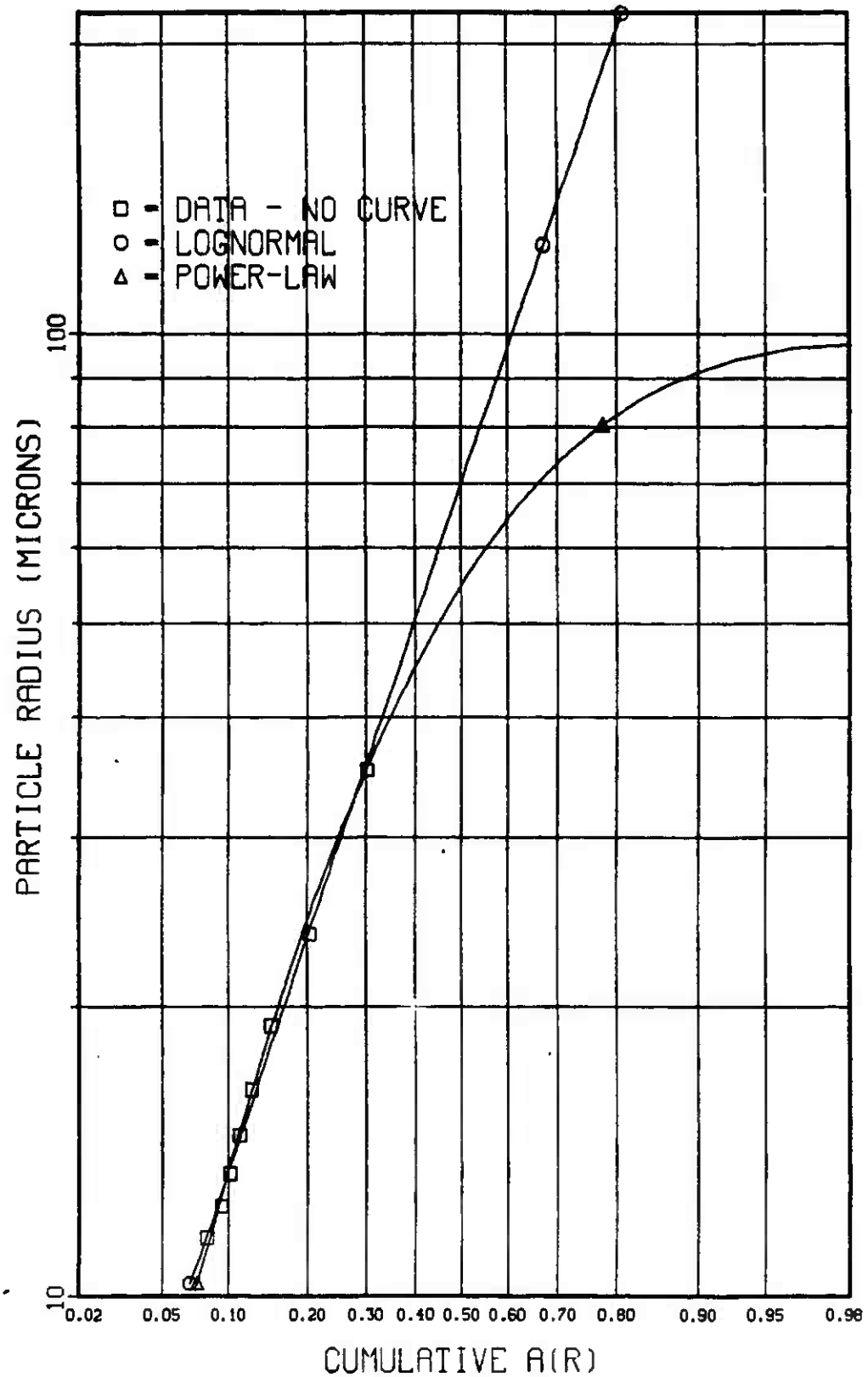

Figure 6: Lognormal and Power-Law Fits to Local Fallout Data
Operation BUSTER-JANGLE Uncle

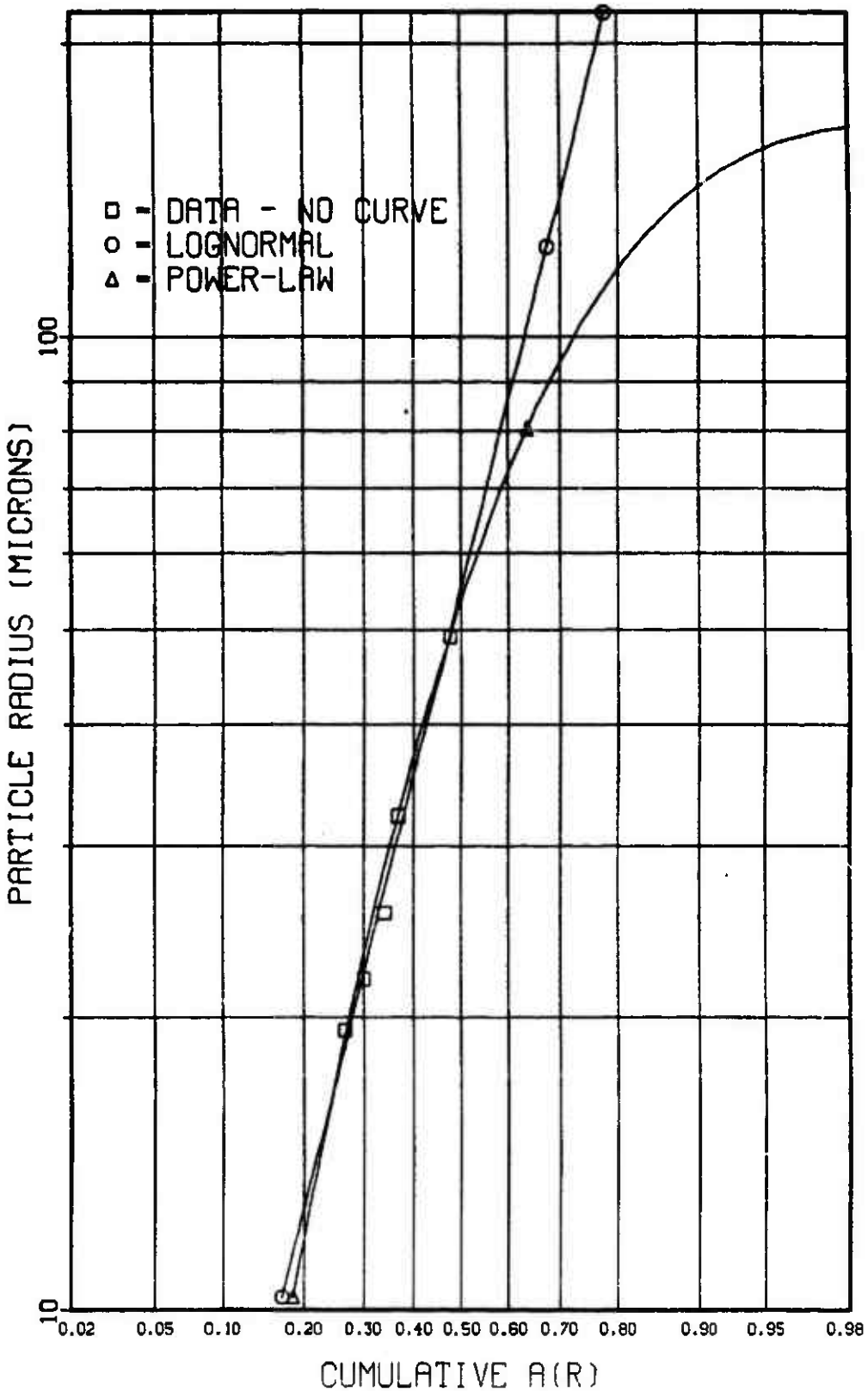

Figure 7: Lognormal and Power-Law Fits to Local Fallout Data
Operation BUSTER-JANGLE Sugar

Two Distributions

For bursts at scaled heights of bursts below 700 feet there is an unlimited set of parameters (r_{m1}, β_1, r_{m2}, β_2, f_t) that will describe the fallout data. One possible choice for these parameters is presented in Table 5 and shown graphically in Figures 8-10 for surface, tower and air bursts. The values presented in Table 5 were obtained by selecting r_{m2} of 0.2 μ and using Baker's distribution, r_m of 0.1 μ and β of ln 2 (2), to represent n_1. Baker's distribution was chosen to represent n_1 because it is in reasonable agreement with the results for the air bursts HARDTACK II Lea and PLUMBBOB Doppler. There is no special significance to this choice of r_{m2} as corresponding values of f_2 and β_2 may be found for other values of r_{m2}. Rather, this table is intended to demonstrate that local fallout from these classes of bursts may be described by a linear combination of two lognormal distributions. Interestingly, the average slope of the second distribution, β_2 of 4.2, is remarkably similar to the slope of DELFIC default distribution (Table 1) for land surface detonations.

As expected, Figure 11 shows that f_2 generally decreases with scaled height of burst. In other words, the fraction of activity carried by device debris increases with scaled height of burst.

It was shown previously that a subsurface burst may be described by a single lognormal distribution. It may also, as Heft suggests (5:256), be described by a linear combination of three lognormal distributions. Eight parameters are required to describe this distribution. Not surprisingly, many sets of such parameters were found. The partitioning of activity among three different distributions is even more uncertain than was the case for above ground bursts.

Discussion

For air bursts the fraction of activity grounded in the time considered never exceeded 0.9%. This is insufficient to make reliable conclusions about the particle size distribution of

Table 5: Lognormal Parameters
(Two Distributions)

$r_{m1} = 0.1\ \mu, \beta_1 = \ln 2$

	Fraction a_2, f_2	Median radius, r_{m2} (μ)	exp (β_2)
Surface			
PLUMBBOB Coulomb-B	0.214	0.2	4.7
BUSTER-JANGLE Sugar	0.924	0.2	4.6
Tower			
TEAPOT Hornet	0.115	0.2	5.2
TEAPOT Bee	0.0282	0.2	6.0
TEAPOT Apple	0.0404	0.2	4.4
PLUMBBOB Shasta	0.0994	0.2	4.8
UPSHOT-KNOTHOLE Nancy	0.0871	0.2	4.3
TEAPOT Apple II	0.0852	0.2	4.1
UPSHOT-KNOTHOLE Harry	0.703	0.2	3.4
UPSHOT-KNOTHOLE Simon	0.195	0.2	3.6
Air			
PLUMBBOB Morgan	0.00583	0.2	4.7
PLUMBBOB Owens	0.0407	0.2	3.2
UPSHOT-KNOTHOLE Grable	0.0240	0.2	3.4
PLUMBBOB Stokes	0.00036	0.2	4.1
PLUMBBOB Priscilla	0.0366	0.2	3.3
PLUMBBOB Hood	0.00212	0.2	4.0

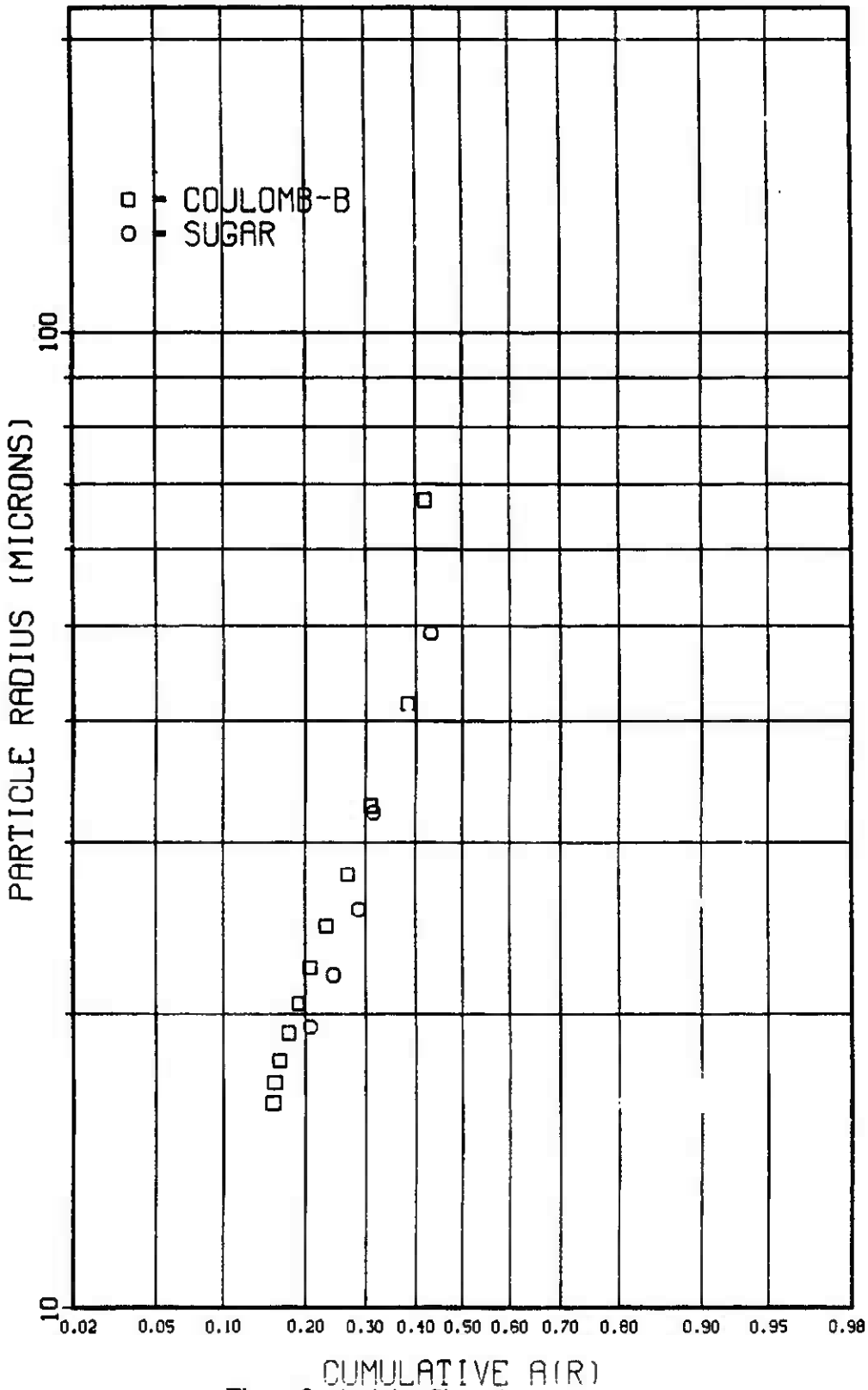

Figure 8: Activity-Size Distribution, a_2
Surface Bursts

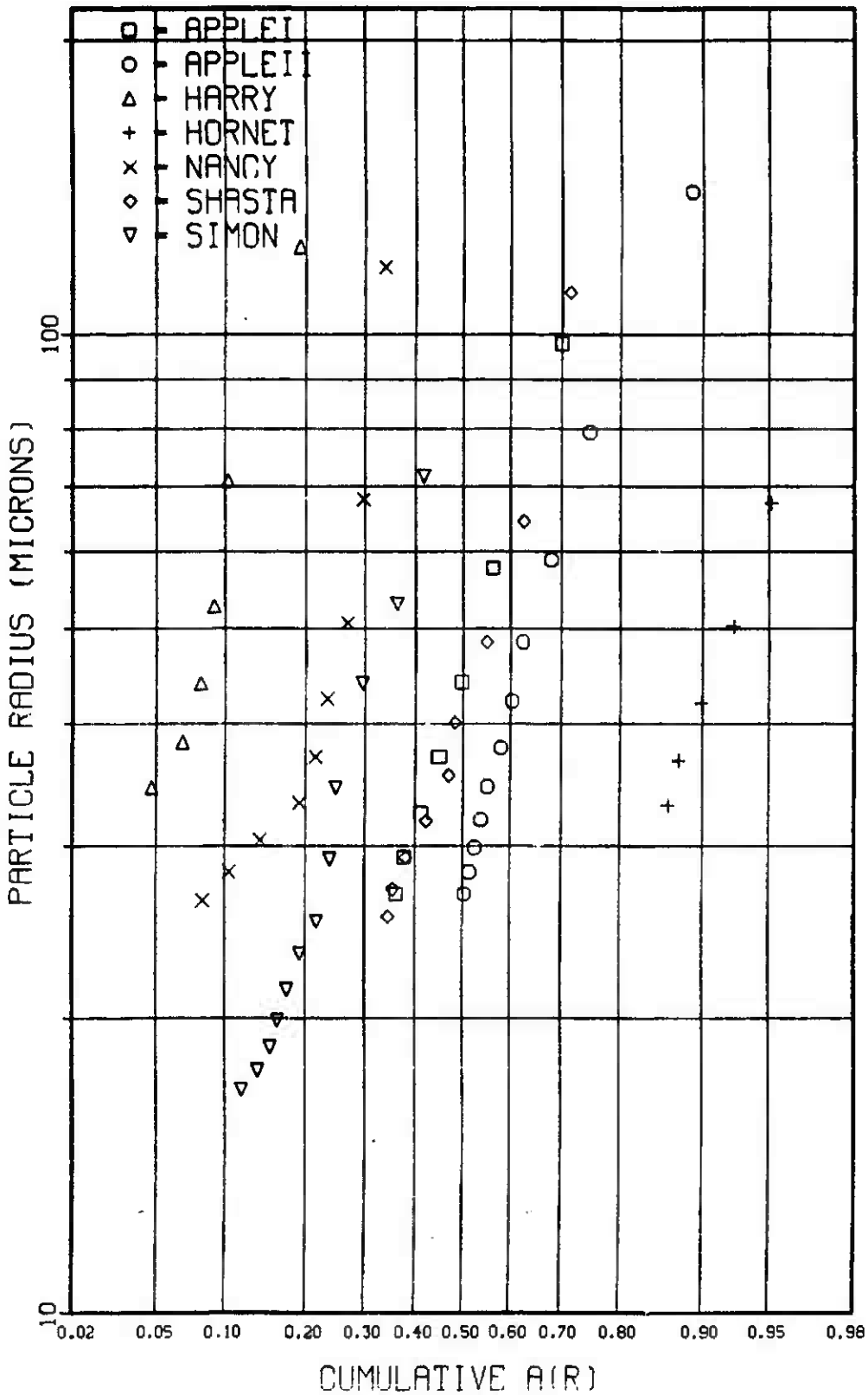

Figure 9: Activity-Size Distribution, a_2
Tower Bursts

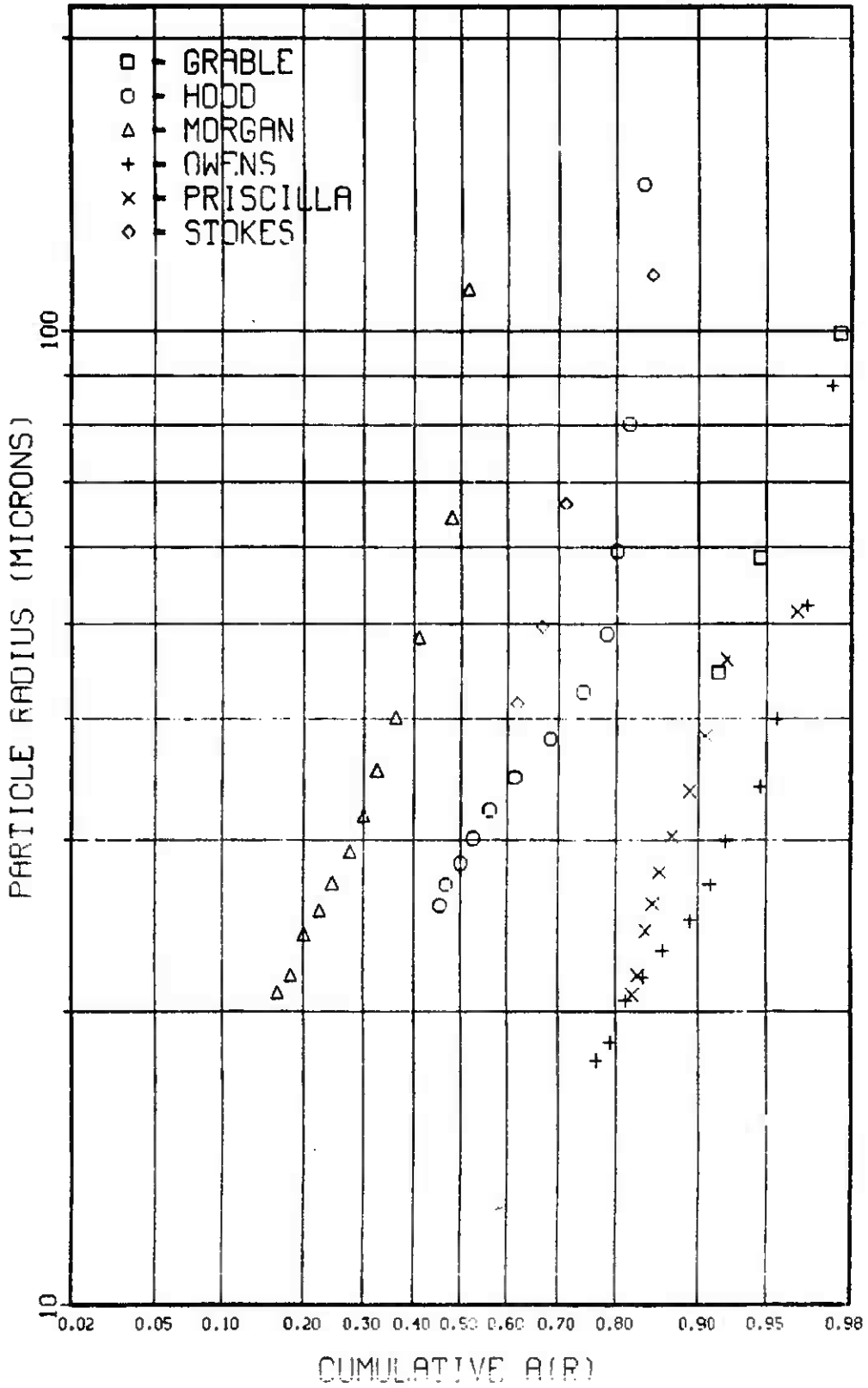

Figure 10: Activity-Size Distribution, a_2
Air Bursts

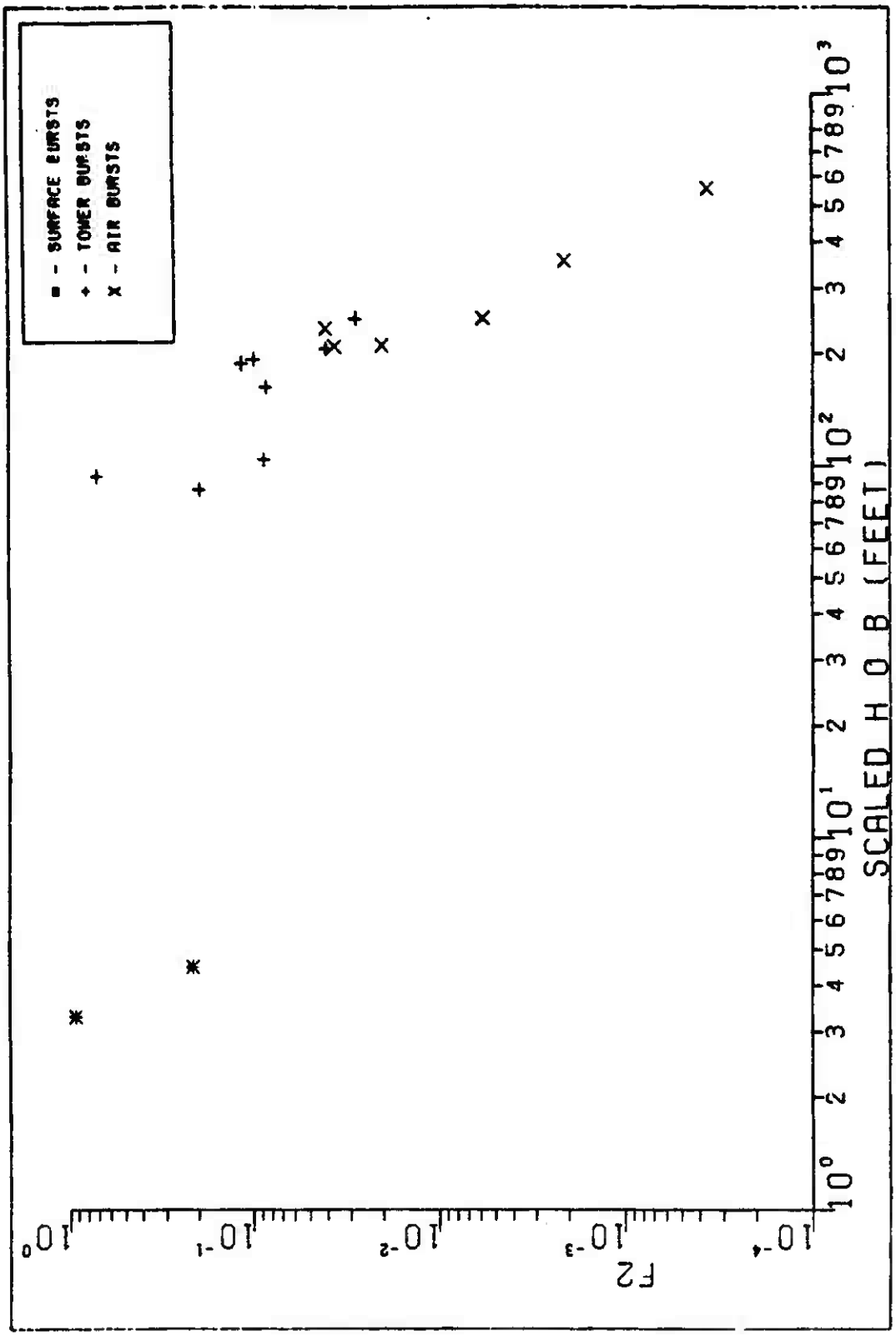

Figure 11: Fraction of Activity on Distribution n_2 vs. Scaled Height of Burst

activity-bearing debris produced by this type of burst. It may be said that, since at 12 hours most particles larger than 20 μ have grounded, more than 99% of the activity is carried by particles smaller than 20 μ. This is consistent with Baker's proposed lognormal distribution for long-term stratospheric debris (2).

Tower bursts produced more fallout than did air bursts by a factor of about ten, but there was still insufficient fallout to make any reliable conclusions about the size distribution of the debris. Any such results would likely be of questionable utility in operational fallout prediction models because of the presence of melted and vaporized tower materials in the radioactive debris. These materials may or may not follow the distribution of debris from an air or surface burst.

If we combine the observations of Heft (10:254) and Yoon (23:3-6) presented on page 7, we might not be surprised that all but three air and tower bursts occurring below a scaled height of burst of approximately 700 feet cannot be reasonably described by a single lognormal distribution function. Interestingly, the two air bursts that could be described by a single lognormal distribution, HARDTACK II Lea (SHOB 1341 feet) and PLUMBBOB Doppler (SHOB 674 feet), were close to or above that altitude. While these distributions seem to be quite different than Baker's distribution (2), all three predict a median radius of the activity distribution, $r_{2.5}$, of within a factor of 2 of 0.5 μ.

In the case of surface and near-surface bursts it appears that, consistent with Heft's observations (10:254), local fallout from these types of bursts may be modeled by a linear combination of two lognormal distributions. The parameters of these distributions are very uncertain as many sets of these parameters will describe the local fallout data. The partition of activity between the two distributions is also uncertain. While Figure 11 shows a definite trend for air and tower bursts, there is no local fallout data in the range of scaled heights of bursts from 5 to 80 feet to yield information on the partitioning of activity in the transition region between surface and air bursts.

The power-law distribution will describe the local fallout data for each of the bursts studied. The exponents, n, found are remarkably consistent within each class of bursts examined; however, in many cases artificially small maximum radii found. Particles much larger than 200 μ have been observed for a large number of bursts all types. This may be corrected by not fixing r_{min} at 0.01 μ. Larger values are then found for all three parameters. But minimum radii are then found to be in the range from 0.5 to 1.0 μ and smaller particles have been observed.

Baker has shown that the r^{-n} distribution observed by Nathans (15) may be a product of the assumed initial spatial distribution of activity in the stabilized cloud (2). He demonstrated that a lognormal particle number-size distribution, distributed normally in the vertical direction, can produce, at times after cloud stabilization, an apparent power-law distribution at sampling altitudes beneath the radioactive cloud. Freiling studied the power-law and lognormal distributions and concluded the difference between these distributions is "trivial" (7:12). Figures 5-7 clearly show that, as Freiling predicts, both a power-law and lognormal distribution may describe the surface and subsurface burst data over the range of particle sizes considered in this study. The lognormal distribution may be preferred because it does not require artificial terminal radii.

It cannot be overemphasized that these results for air and tower bursts are based on a very small fraction of the activity produced by these bursts. The results presented in Table 5 for surface, tower and air bursts are based on one choice for r_{m1}, r_{m2} and β_1 and are not intended to be the definitive values. Other choices are certainly possible and would be equally valid. Likewise, no one set of parameters can be chosen for subsurface bursts. One must conclude that local fallout data alone is not enough to determine the values of these parameters.

Implications

If Heft's multi-distribution model is correct as this research suggests, then there are some obvious implications for local fallout modeling. If Baker's distribution, or some similar distribution, correctly describes the vaporized soil and bomb debris, then this class of particles will not contribute significantly to local fallout. Local fallout would then be produced almost exclusively by the second class of particles, the unvaporized soil.

This suggests two options for modeling local fallout. One method would be to explicitly consider two distribution functions. The other approach would be to ignore the bomb debris and vaporized soil and consider only the unvaporized soil. The source normalization constant may then be adjusted to account for only the fraction of activity available for local fallout, i.e. the activity carried by the unvaporized soil. This is essentially what is done by models that use smaller source normalization constants, Table 2, than the lower bound on that quantity proposed in Chapter 4.

Since the first distribution does not contribute to local fallout, the extent of local fallout will be strongly dependent on the fraction of activity carried by the second distribution. As can be seen in Figure 11, this partitioning of activity between the two distributions is a strong function of scaled height of burst. This relationship and the parameters of the distribution functions need to be better understood in order to predict local fallout with confidence.

VI. Conclusions

Iso-dose rate contours from atmospheric nuclear tests were integrated to obtain information about the size distribution of nuclear debris. Several assumptions were made to extract a number-size distribution from the fallout data.

Air and tower bursts produced insufficient local fallout to make any determinations about the size distribution of particles produced by these types of bursts.

Surface and subsurface bursts may be modeled by a single lognormal distribution, a linear combination of two or more lognormal distributions, or a power-law distribution. The power-law distribution may require an artificially large r_{max} or small r_{min} and is not preferred.

The local fallout data did not yield conclusive information on the parameters of the size distribution of nuclear debris. The nature of the distribution function was not established but a linear combination of lognormal distributions holds the most promise. The evidence suggests that most of the activity produced by an air burst, more than 99%, is carried by particles smaller than 20 μ. For surface and shallow subsurface bursts approximately half of the activity is carried by particles smaller than about 60 μ.

Bursts below a scaled height of burst of 700 feet might be described by a linear combination of two lognormal distribution functions. The bomb debris and vaporized soil might be defined by a small median radius and geometric standard deviation. Baker's distribution, r_m of 0.1 μ and β of ln 2, is one such distribution. Soil entrained in the fireball but not vaporized might be defined by larger parameters, e.g. the DELFIC distribution, r_m of 0.204 μ and β of ln 4. The fraction of activity carried by the latter distribution decreases rapidly with scaled height of burst. Bursts above a scaled height of burst of 700 feet might be described by a single lognormal distribution, e.g. Baker's distribution.

The source normalization constant, including the surface roughness factor, was found to be at least 2210 r-mi^2/hr-kt for the Nevada Test Site. This is significantly larger than several

previously reported values.

It is believed that further study of the particle size distribution question is warranted. The method used in this research holds little promise given the narrow range of particle sizes over which information may be obtained, from about 15 to 140 μ, and the tremendous uncertainty in the data. Further study of cloud and ground samples, using modern ashing, separation and microscopy techniques, would likely be more fruitful.

References

1. Aitchson, J. and Brown, J. A. C. The Lognormal Distribution. Cambridge: Cambridge University Press (1957).

2. Baker, George H., AFIT doctoral student, "The Implications of Atmospheric Test Fallout Data for Modeling Nuclear Winter." Department of Engineering Physics Doctoral Seminar (To be published in PhD Dissertation, 1987). Air Force Institute of Technology (AU), Wright-Patterson Air Force Base OH, 5 and 12 November 1986.

3. Bridgman, Charles J. "Course Notes," NE6.35, Residual Effects of Nuclear Weapons. School of Engineering, Air Force Institute of Technology (AU), Wright-Patterson Air Force Base OH.

4. Bridgman, Charles J. and Bigelow, Winfield S. "A New Fallout Prediction Model," Health Physics, 43, 205-218 (August 1982).

5. Conners, Capt Steven P. Aircrew Dose and Engine Dust Ingestion from Nuclear Cloud Penetration. M. S. Thesis, AFIT/GNE/PH/85M-4. School of Engineering, Air Force Institute of Technology (AU), Wright-Patterson Air Force Base OH, March 1985 (AD-A159246).

6. Freiling, E. C. "Radionuclide Fractionation in Bomb Debris," Science, 133, 1991-1998 (June 1961).

7. ----- A Comparison of the Fallout Mass-Size Distributions Calculated by Lognormal and Power-Law Models. USNRDL-TR-1105. U. S. Naval Radiological Defense Laboratory, San Francisco CA, 14 November 1966 (AD-646019).

8. Freiling, E. C. and Rainey, S. C. Fractionation II. On Defining the Surface Density of Contamination. USNRDL-TP-631. U. S. Naval Radiological Defense Laboratory, San Francisco CA, 13 March 1963 (AD-402293).

Though not directly referenced in this report, the reader may find the other volumes of this series to be of interest. These are:

Freiling, E. C. Fractionation I. High-Yield Surface Burst Correlation. USNRDL-TR-385. U. S. Naval Radiological Defense Laboratory, San Francisco CA, 29 October 1959 (AD-232085).

Freiling, E. C. Fractionation III. Estimation of Degree of Fractionation and Radionuclide Partition for Nuclear Debris. USNRDL-TR-680. U. S. Naval Radiological Defense Laboratory, San Francisco CA, 18 September 1963 (AD-423725).

Freiling, E. C. Fractionation IV. Illustrative Calculations of the Effect of Radionuclide Fractionation on Exposure-Dose Rate from Local Fallout. USNRDL-TR-715. U. S. Naval Radiological Defense Laboratory, San Francisco CA, 6 January 1964 (AD-431227).

9. Glasstone, Samuel and Dolan, Philip J., ed, The Effects of Nuclear Weapons, Third Edition. Washington: U. S. Government Printing Office, 1977.

10. Hawthorne, Howard A., ed, Compilation of Local Fallout Data from Test Detonations 1945-1962 Extracted from DASA 1251 Volume I - Continental U. S. Tests. DNA 1251-1-Ex. Defense Nuclear Agency, Washington DC, 1 May 1979.

11. Heft, Robert E. "The Characterization of Radioactive Particles from Nuclear Weapons Tests," in Radionuclides in the Environment, Advances in Chemistry Series, 93, American Chemical Society: 352-380 (1970).

12. IMSL Library, Volume 3 - FORTRAN Subroutines for Mathematics and Statistics. International Mathematical and Statistical Libraries, Inc., Houston TX, June 1982.

13. Larson, K. H. et al Distribution, Characteristics, and Biotic Availability of Fallout, Operation Plumbbob. WT-1488. Laboratory of Nuclear Medicine and Radiation Biology, The University of California at Los Angeles, Los Angeles CA, 26 July 1966.

14. Nathans, Marcel W. Private communication to George H. Baker, doctoral student, Air Force Institute of Technology (AU), Wright-Patterson Air Force Base OH, 1986.

15. Nathans, Marcel W. et al "The Particle Size Distribution of Nuclear Cloud Samples," in Radionuclides in the Environment, Advances in Chemistry Series, 93, American Chemical Society: 254-281 (1970).

16. Nathans, Marcel W. et al "Particle Size distribution in Clouds from Nuclear Air Bursts," Journal of Geophysical Research, 75, American Geophysical Union: 7559-7572 (December 1970).

17. Seery, C. J. and Polan, M. An Analysis of the Fallout Prediction Models, Volume II: Analysis, Comparison and Evaluation of Model Predictions. NRDL-TRC-68-59, Contract N228(62479)62185. Ford Instrument Division, Sperry Rand Corporation, Long Island City NY, August 1968 (AD-843390).

18. Tompkins, Robert C. Department of Defense Land Fallout Prediction System (DELFIC), Volume V - Particle Activity. DASA-1800-V, NDL-TR-102. U. S. Army Ballistic Research Laboratories, Aberdeen Proving Ground MD, February 1968 (AD-832239).

19. ----- Effect of Depth of Burial on Fallout From Atomic Demolition Munitions. Memorandum Report No. 2317. U. S. Army Ballistic Research Laboratories, Aberdeen Proving Ground MD, August 1973 (AD-913911).

20. Turco, Richard A. et al Global Atmospheric Consequences of Nuclear War. Unpublished report. R & D Associates, Marina del Rey CA, March 1983.

21. U. S. Standard Atmosphere, 1976. National Oceanic and Atmospheric Administration, National Aeronautics and Space Administration and U. S. Air Force, Washington DC, 1976.

22. Valley, Shea L., ed Handbook of Geophysics and Space Environments. Office of Aerospace Research, Air Force Cambridge Research Laboratories, Bedford MA, 1965.

23. Yoon, Barbara L. et al Nuclear Dust and Radiation Cloud Environments for Aircraft and Optical Sensors. Contract DNA-001-85-C-0022. R & D Associates, Marina del Rey CA, April 1985.

Appendix A - Tests Studied

Series	Shot	Yield (kt) (10)
Subsurface Bursts		
TEAPOT	Ess	1
BUSTER-JANGLE	Uncle	1.2
Surface Bursts		
PLUMBBOB	Coulomb B	0.3
BUSTER-JANGLE	Sugar	1.2
Tower Bursts		
TEAPOT	Hornet	4
TEAPOT	Bee	8
TEAPOT	Apple	14
PLUMBBOB	Shasta	17
TEAPOT	Met	22
UPSHOT-KNOTHOLE	Nancy	24
TEAPOT	Apple II	29
UPSHOT-KNOTHOLE	Harry	32
UPSHOT-KNOTHOLE	Simon	43

Series	Shot	Yield (kt) (10)
Air Bursts		
HARDTACK II	Lea	1.4
PLUMBBOB	Morgan	8
PLUMBBOB	Owens	9.7
PLUMBBOB	Doppler	11
UPSHOT-KNOTHOLE	Grable	15
PLUMBBOB	Stokes	19
PLUMBBOB	Priscilla	37
PLUMBBOB	Hood	74

These tests were selected utilizing the following criteria:

1. Well-behaved iso-dose rate contours and arrival time curves.

2. Availability of data on burst conditions, e.g. yield, height of burst, cloud dimensions, test environment (tower, balloon, surface, subsurface).

3. Selection of a wide range of yields and heights of burst.

Appendix B: Results of Contour Integration

This appendix contains the results of the numerical integration of the iso-dose contours for each burst studied. The results appear in the same sequence as the bursts were listed in Appendix A.

The header information, i.e. yield, cloud dimensions, and heights of burst, was obtained from reference (10). The scaled heights of burst were found using equation (11). Cloud bottom heights in parentheses were estimated from the dimensions of similar bursts.

Time is the arrival time of fallout in hours. r (t) is the radius, in microns, of particles falling to ground at time t from the bottom of the visible cloud. J (t) is the result of the numerical integration of the contours out to arrival time t. G (t) is found by dividing J (t) by the effective source normalization constant K, taken here to be 2350 r-mi^2/hr-kt (4:208), and the fission yield of the weapon in kilotons.

Shot: Ess

Yield: 1 Kiloton

Cloud Bottom Height: (feet) (9000) Height of Burst: (feet) -67

Cloud Top Height: (feet) 12500 Scaled HOB: (feet) -67

Time (hr)	r (t) (μ)	J (t) (r-mi^2/hr)	G (t)
1	39.2	2020.5	0.860
2	26.7	2075.0	0.883
3	21.4	2114.4	0.900
4	18.4	2149.2	0.915
5	16.4	2173.8	0.925
6	14.9	2185.1	0.930
7	13.8	2194.1	0.934
8	12.9	2201.7	0.937
9	12.1	2208.4	0.940
10	11.5	2212.9	0.942

Shot: Uncle

Yield: 1.2 Kilotons

Cloud Bottom Height: (feet) (8000) Height of Burst: (feet) -17

Cloud Top Height: (feet) 11500 Scaled HOB: (feet) -16

Time (hr)	r (t) (μ)	J (t) (r-mi^2/hr)	G (t)
1	35.2	1968.2	0.698
2	23.8	2244.8	0.797
3	19.1	2403.1	0.852
4	16.4	2469.6	0.876
5	14.7	2506.6	0.889
6	13.4	2532.8	0.898
7	12.4	2556.1	0.906
8	11.5	2593.5	0.920

Shot: Sugar

Yield: 1.2 Kilotons

Cloud Bottom Height: (feet)	11000	Height of Burst: (feet)	3.5
Cloud Top Height: (feet)	15000	Scaled HOB: (feet)	3.3

Time (hr)	r (t) (μ)	I (t) (r-mi^2/hr)	G (t)
1	49.2	1483.3	0.526
2	32.2	1783.6	0.632
3	25.6	1856.4	0.658
4	21.9	1970.4	0.699
5	19.4	2066.6	0.733

Shot: Coulomb B

Yield: 0.3 Kilotons

Cloud Bottom Height: (feet) (15000) Height of Burst: (feet) 3

Cloud Top Height: (feet) 18000 Scaled HOB: (feet) 4.5

Time (hr)	r (t) (μ)	J (t) (r-mi^2/hr)	G (t)
1	67.3	87.6	0.124
2	41.6	93.2	0.132
3	32.7	103.9	0.147
4	27.8	110.3	0.156
5	24.6	115.8	0.164
6	22.3	119.5	0.170
7	20.5	122.3	0.174
8	19.1	124.4	0.176
9	17.9	126.2	0.179
10	17.0	127.2	0.180
11	16.2	127.5	0.181

Shot: Hornet

Yield: 4 Kilotons

Cloud Bottom Height: (feet)	27800	Height of Burst: (feet)	300
Cloud Top Height: (feet)	37000	Scaled HOB: (feet)	189

Time (hr)	r (t) (μ)	I (t) (r-mi^2/hr)	G (t)
1	117.2	715.5	0.076
2	67.8	759.7	0.081
3	50.7	791.7	0.084
4	42.4	828.8	0.088
5	37.0	850.2	0.090
6	33.2	876.4	0.093
7	30.4	932.3	0.099
8	28.2	969.2	0.103
9	26.4	994.4	0.106

Shot: Bee

Yield: 8 Kilotons

Cloud Bottom Height: (feet)	29500	Height of Burst: (feet)	500
Cloud Top Height: (feet)	39700	Scaled HOB: (feet)	250

Time (hr)	r (t) (μ)	I (t) (r-mi^2/hr)	G (t)
1	123.0	428.1	0.023
2	70.8	474.7	0.025
3	52.7	481.0	0.026
4	44.0	487.0	0.026
5	38.3	494.0	0.026
6	34.4	504.2	0.027

Shot: Apple I

Yield: 14 Kilotons

Cloud Bottom Height: (feet)	22600	Height of Burst: (feet)	500
Cloud Top Height: (feet)	32000	Scaled HOB: (feet)	207

Time (hr)	r (t) (μ)	J (t) (r-mi^2/hr)	G (t)
1	97.9	399.0	0.012
2	57.7	582.0	0.018
3	44.1	669.6	0.020
4	37.0	733.2	0.022
5	32.4	781.5	0.024
6	29.2	827.7	0.025
7	26.8	848.7	0.026

Shot: Shasta

Yield: 17 Kilotons

Cloud Bottom Height: (feet)	16000	Height of Burst: (feet)	500
Cloud Top Height: (feet)	32000	Scaled HOB: (feet)	194

Time (hr)	r (t) (μ)	I (t) (r-mi^2/hr)	G (t)
1	71.6	2310.7	0.058
1.5	53.0	2529.6	0.063
2	44.0	2795.0	0.070
3	34.4	2984.7	0.075
4	29.1	3018.9	0.076
5	25.1	3106.1	0.078
6	23.3	3208.8	0.080
7	21.4	3281.6	0.082
8	19.9	3331.6	0.083
9	18.7	3368.1	0.084
10	17.7	3429.2	0.086
11	16.9	3503.7	0.088

Shot: Met

Yield: 22 Kilotons

Cloud Bottom Height: (feet)	31800	Height of Burst: (feet)	400
Cloud Top Height: (feet)	40300	Scaled HOB: (feet)	143

Time (hr)	r (t) (μ)	I (t) (r-mi^2/hr)	G (t)
1	130.9	151.5	0.003
2	74.9	421.8	0.008
3	55.3	867.1	0.017
4	46.1	1583.1	0.031
5	39.8	1845.6	0.036
6	36.0	2031.7	0.039

Shot: Nancy

Yield: 24 Kilotons

Cloud Bottom Height: (feet)	26000	Height of Burst: (feet)	300
Cloud Top Height: (feet)	41500	Scaled HOB: (feet)	104

Time (hr)	r (t) (μ)	I (t) (r-mi^2/hr)	G (t)
1	110.5	1393.1	0.025
2	64.4	1834.0	0.033
3	48.5	2209.3	0.039
4	40.1	2542.2	0.045
5	35.4	2606.9	0.046
7	31.8	2832.0	0.050
8	29.2	3041.8	0.054
9	27.1	3164.9	0.056
10	25.4	3208.3	0.057

Shot: Apple II

Yield: 29 Kilotons

Cloud Bottom Height: (feet)	34500	Height of Burst: (feet)	500
Cloud Top Height: (feet)	51000	Scaled HOB: (feet)	163

Time (hr)	r (t) (μ)	I (t) (r-mi^2/hr)	G (t)
1	140.0	613.2	0.009
2	79.5	1382.5	0.020
3	58.8	1775.3	0.026
4	48.5	2085.5	0.031
5	42.2	2206.6	0.032
6	37.8	2333.9	0.034
7	34.5	2490.1	0.037
8	31.9	2567.7	0.038
9	29.9	2638.8	0.039
10	28.2	2700.9	0.040
11	26.8	2758.5	0.040

Shot: Harry

Yield: 32 Kilotons

Cloud Bottom Height: (feet)	27500	Height of Burst: (feet)	300
Cloud Top Height: (feet)	42500	Scaled HOB: (feet)	94

Time (hr)	r (t) (μ)	I (t) (r-mi^2/hr)	G (t)
2	67.2	2577.2	0.034
3	50.3	3860.9	0.051
4	42.0	5308.9	0.071
5	36.7	6593.8	0.088
6	33.0	7184.8	0.096

Shot: Simon

Yield: 43 Kilotons

Cloud Bottom Height: (feet)	31000	Height of Burst: (feet)	300
Cloud Top Height: (feet)	44000	Scaled HOB: (feet)	86

Time (hr)	r (t) (μ)	I (t) (r-mi^2/hr)	G (t)
1	128.2	7102.8	0.070
2	73.5	9364.7	0.093
3	54.6	10770.6	0.107
4	45.4	11635.5	0.115
5	39.3	12592.5	0.125
6	35.5	13413.9	0.133
7	32.4	14033.9	0.139
8	30.0	14212.1	0.141
9	28.1	14228.1	0.141
10	26.6	14235.1	0.141

Shot: Lea

Yield: 1.4 Kilotons

Cloud Bottom Height: (feet)	12000	Height of Burst: (feet)	1500
Cloud Top Height: (feet)	17000	Scaled HOB: (feet)	1341

Time (hr)	r (t) (μ)	I (t) (r-mi^2/hr)	G (t)
2	34.8	1.45	0.000
3	27.5	1.52	0.000
4	23.5	1.88	0.001
5	20.9	2.88	0.001
6	18.9	4.46	0.001
7	17.4	5.91	0.002
8	16.3	8.09	0.002
9	15.3	10.87	0.003
10	14.5	13.40	0.004
11	13.8	15.97	0.005
12	13.2	18.45	0.006
13	12.7	20.81	0.006

Shot: Morgan

Yield: 8 Kilotons

Cloud Bottom Height: (feet)	26000	Height of Burst: (feet)	500
Cloud Top Height: (feet)	40000	Scaled HOB: (feet)	250

Time (hr)	r (t) (μ)	J (t) (r-mi^2/hr)	G (t)
1	110.5	53.21	0.003
2	64.4	57.10	0.003
3	48.5	64.64	0.003
4	40.1	69.91	0.004
5	35.4	74.00	0.004
6	31.8	76.68	0.004
7	29.2	79.42	0.004
8	27.1	82.66	0.004
9	25.4	84.95	0.005
10	24.0	87.66	0.005

Shot: Owens

Yield: 9.7 Kilotons

Cloud Bottom Height: (feet)	20000	Height of Burst: (feet)	500
Cloud Top Height: (feet)	35000	Scaled HOB: (feet)	234

Time (hr)	r (t) (μ)	I (t) (r-mi^2/hr)	G (t)
1	87.9	21.21	0.001
2	52.2	28.97	0.001
3	39.9	41.44	0.002
4	34.0	49.71	0.002
5	29.9	70.98	0.003
6	27.0	82.86	0.004
7	24.8	99.56	0.004
8	23.1	127.13	0.006
9	21.7	149.79	0.007
10	20.5	172.24	0.008
11	21.8	193.31	0.008
12	20.9	214.17	0.009

Shot: Doppler

Yield: 11 Kilotons

Cloud Bottom Height: (feet) 23000 Height of Burst: (feet) 1500

Cloud Top Height: (feet) 28000 Scaled HOB: (feet) 674

Time (hr)	r (t) (μ)	I (t) (r-mi^2/hr)	G (t)
1	99.4	1.73	0.000
2	58.5	1.82	0.000
3	44.6	2.02	0.000
4	37.4	2.42	0.000
5	32.4	3.62	0.000
6	29.5	5.57	0.000
7	27.1	9.53	0.000
8	25.2	13.46	0.001
9	23.6	19.19	0.001
10	22.3	30.86	0.001
11	21.2	50.05	0.002
12	20.2	70.11	0.003
13	19.4	88.22	0.003
14	18.7	108.79	0.004

Shot: Grable

Yield: 15 Kilotons

Cloud Bottom Height: (feet)	23000	Height of Burst: (feet)	524
Cloud Top Height: (feet)	35000	Scaled HOB: (feet)	212

Time (hr)	r (t) (μ)	I (t) (r-mi^2/hr)	G (t)
1	99.4	17.38	0.000
2	58.5	45.32	0.001
3	44.6	70.25	0.002

Shot: Stokes

Yield: 19 Kilotons

Cloud Bottom Height: (feet)	27000	Height of Burst: (feet)	1500
Cloud Top Height: (feet)	37000	Scaled HOB: (feet)	562

Time (hr)	r (t) (μ)	I (t) (r-mi^2/hr)	G (t)
1	114.2	2.41	0.000
2	66.5	4.58	0.000
3	49.7	5.28	0.000
4	41.4	6.10	0.000

Shot: Priscilla

Yield: 37 Kilotons

Cloud Bottom Height: (feet)	24000	Height of Burst: (feet)	700
Cloud Top Height: (feet)	43000	Scaled HOB: (feet)	210

Time (hr)	r (t) (μ)	I (t) (r-mi^2/hr)	G (t)
3	46.0	243.2	0.003
4	38.4	299.1	0.003
5	33.7	342.6	0.004
6	30.3	404.2	0.005
7	27.8	446.2	0.005
8	25.8	473.6	0.005
9	24.2	501.5	0.006
10	21.8	537.2	0.006
11	20.8	560.4	0.006

Shot: Hood

Yield: 74 Kilotons

Cloud Bottom Height: (feet)	48000	Height of Burst: (feet)	1500
Cloud Top Height: (feet)	35000	Scaled HOB: (feet)	357

Time (hr)	r (t) (μ)	I (t) (r-mi^2/hr)	G (t)
1	141.6	59.3	0.000
2	80.3	66.3	0.000
3	59.4	73.0	0.000
4	48.9	79.1	0.000
5	42.6	93.6	0.001
6	38.1	115.6	0.001
7	34.8	141.3	0.001
8	32.2	160.9	0.001
9	30.1	173.8	0.001
10	28.4	183.4	0.001
11	27.0	194.9	0.001
12	25.7	199.3	0.001

Vita

Captain Norman C. Davis

He attended the University of Southern California from which he received the degree of Bachelor of Science in Chemical Engineering in December 1981. Upon graduation, he received a commission in the U. S. Marine Corps and attended The Basic School and Infantry Officers' Course in Quantico, Virginia. He then served as a rifle platoon commander, battalion S-1/Adjutant and Dragon missile platoon commander with the 3d Battalion, 3d Marines, and as Regimental Mess Hall Officer with the 3d Marine Regiment (Rein.), 1st Marine Brigade, FMF, until entering the School of Engineering, Air Force Institute of Technology, in August 1985.

UNCLASSIFIED
SECURITY CLASSIFICATION OF THIS PAGE

AD-A179 114

REPORT DOCUMENTATION PAGE

Form Approved OMB No. 0704-0188

1a. REPORT SECURITY CLASSIFICATION UNCLASSIFIED	1b. RESTRICTIVE MARKINGS
2a. SECURITY CLASSIFICATION AUTHORITY	3. DISTRIBUTION/AVAILABILITY OF REPORT Approved for public release; distribution unlimited
2b. DECLASSIFICATION/DOWNGRADING SCHEDULE	
4. PERFORMING ORGANIZATION REPORT NUMBER(S) AFIT/GNE/ENP/86D-1	5. MONITORING ORGANIZATION REPORT NUMBER(S)
6a. NAME OF PERFORMING ORGANIZATION School of Engineering	6b. OFFICE SYMBOL (If applicable) AFIT/ENP
6c. ADDRESS (City, State, and ZIP Code) Air Force Institute of Technology Wright-Patterson AFB, Ohio 45433	7a. NAME OF MONITORING ORGANIZATION
8a. NAME OF FUNDING/SPONSORING ORGANIZATION	8b. OFFICE SYMBOL (If applicable)
8c. ADDRESS (City, State, and ZIP Code)	9. PROCUREMENT INSTRUMENT IDENTIFICATION NUMBER
	10. SOURCE OF FUNDING NUMBERS PROGRAM ELEMENT NO. / PROJECT NO. / TASK NO / WORK UNIT ACCESSION NO.
7b. ADDRESS (City, State, and ZIP Code)	

11. TITLE (Include Security Classification)
See Block 19

12. PERSONAL AUTHOR(S)
Norman C. Davis, Captain, U. S. Marine Corps

13a. TYPE OF REPORT	13b. TIME COVERED	14. DATE OF REPORT (Year, Month, Day)	15. PAGE COUNT
M. S. Thesis	FROM _____ TO _____	1986 December	69

16. SUPPLEMENTARY NOTATION

17. COSATI CODES			18. SUBJECT TERMS (Continue on reverse if necessary and identify by block number)
FIELD	GROUP	SUB-GROUP	Local Fallout, Particle Size Distribution Source Normalization Constant

19. ABSTRACT (Continue on reverse if necessary and identify by block number)

Title: PARTICLE SIZE DETERMINATION FROM LOCAL FALLOUT

Thesis Chairman: Charles J. Bridgman, Ph.D.
Professor of Nuclear Engineering
Department of Engineering Physics

Abstract continued on reverse.

Approved for public release: IAW AFR 190-1.
LYNN E. WOLAVER 7 April 87
Dean for Research and Professional Development
Air Force Institute of Technology (AU)
Wright-Patterson AFB OH 45433

20. DISTRIBUTION/AVAILABILITY OF ABSTRACT ☐ UNCLASSIFIED/UNLIMITED ☒ SAME AS RPT. ☐ DTIC USERS	21. ABSTRACT SECURITY CLASSIFICATION UNCLASSIFIED
22a. NAME OF RESPONSIBLE INDIVIDUAL Charles J. Bridgman, Ph.D.	22b. TELEPHONE (Include Area Code) (513) 255-4498 / 22c. OFFICE SYMBOL AFIT/ENP

DD Form 1473, JUN 86 Previous editions are obsolete. SECURITY CLASSIFICATION OF THIS PAGE

UNCLASSIFIED

Block 19. Abstract (cont'd)

Iso-dose rate contours and cloud arrival time data from atmospheric nuclear tests conducted at the Nevada Test Site were examined to validate size distributions currently used in fallout prediction models or to propose new size distributions. There was insufficient local fallout from air and tower bursts to make conclusive determinations about the particle size distributions produced by these types of bursts. The debris produced by surface and shallow subsurface bursts may be described by a lognormal distribution, a power-law distribution, or a linear combination of these or possibly other distribution functions. Additionally, a lower bound of 2210 r-mi^2/hr-kt was established for the source normalization constant.